

Quasiperiodic Fresnel atom optics, focusing, and the quasi-Talbot effect

J. L. Cohen, B. Dubetsky, and P. R. Berman

Department of Physics, University of Michigan, Ann Arbor, Michigan 48109-1120

(Received 24 May 1999)

We propose a laser field configuration that acts as a quasiperiodic atom optical diffraction grating. Exact analytical results for the atomic center-of-mass wave function in the Fresnel region after the grating reveal a quasiperiodic density pattern, a semiclassical focusing effect, and a quasiperiodic self-imaging of the atomic wave function analogous to a Talbot effect. The high-contrast quasiperiodic pattern that forms at the focal plane survives both transverse and longitudinal velocity averaging. The quasi-Talbot effect should be observable using atoms from Bose-Einstein condensates. [S1050-2947(99)00111-0]

PACS number(s): 03.75.Be, 39.20.+q, 32.80.Lg

I. INTRODUCTION

Increased attention has been given to periodic atom optical systems and to drawing parallels between solid-state physics and the corresponding atom optics in an easily controlled environment [1]. Periodic atom optical elements have been used for spatial- [2] and time-domain [3,4] interferometry, atom focusing and lithography [5,6], Bragg scattering [7], anomalous transmission and frequency-shifting Bragg gratings [8], as well as to exhibit Fresnel diffraction and the self-imaging (Talbot effect [9]) of an atomic wave packet [10]. In addition, optical lattices [11] and atoms interacting with modulated standing waves have been used to simulate solid-state effects using atomic de Broglie waves. These atoms can exhibit structural effects, such as quantized motion [12] and extended/localized state (metal/insulatorlike) transitions [13], as well as dynamical effects, such as quantum momentum diffusion and a transition toward chaos [14], propagation of elementary excitations [15], site-to-site transport [16], Bloch oscillations [17], Wannier-Stark ladders [18], and wave-packet localization dynamics and oscillations [19].

Much of the previous work on quasiperiodic systems, particularly in the physics community as opposed to the mathematics community, has concentrated on discrete systems [20–22]. Typically, a quasiperiodic potential is defined on top of a discrete quasiperiodic lattice (like the Harper model). Within the standard Harper model, the discrete Hamiltonian has two terms, a site-to-site hopping term that represents the kinetic and potential energies on the underlying lattice and a potential term with an incommensurate period compared to the lattice that takes on a quasiperiodic sequence of values at each successive site. Articles discussing the Harper model are ubiquitous in this subfield of condensed matter [20–24]. Alternatively, in order to model condensed-matter experiments, a layered system of fixed thickness has been considered with quasiperiodic stacking sequences of different species, or a two-species solid has been studied with the thickness of the layers forming a quasiperiodic sequence [20]. A common quasiperiodic sequence used is the Fibonacci series, which is not unrelated to converging sequences that approximate the incommensurate wave-vector ratio chosen for this work ($\sqrt{2}$). To further the connection of atom optics with condensed matter and classical optics (where far-field quasiperiodic diffraction patterns

have been observed [25]), the extension of atom optical experiments to quasiperiodic systems seems natural.

Real systems in condensed matter and especially atom optics must be understood quantitatively as continuous systems. The full Hamiltonian consisting of the kinetic energy and two or more potentials that have incommensurate periods must be considered. Recently, Guidoni and co-workers [26] trapped cesium atoms into a quasiperiodic optical lattice formed by a three-dimensional laser configuration with incommensurate spatial components of intensity. Georgakis and co-workers have been analyzing such optical lattices to understand their eigenstructure and their relationship with quasiperiodic condensed-matter systems in one (1D) and two dimensions (2D) [27]. Recently, we proposed to extend atom lithography and interferometry experiments to create atomic beams or cold trapped atoms with quasiperiodic center-of-mass wave functions [28]. This paper details our scheme for such an experiment. In Sec. II we present exact analytical results for the atomic wave function and density in the Fresnel region after an interaction with a 1D, quasiperiodic atom optical diffraction grating. Fourier analysis reveals the quasiperiodic nature of the wave packets and facilitates an average over atomic velocity distributions. In Sec. III we study the focusing effect that results from the quasiperiodic phase modulation of the wave function, leading to a high-contrast quasiperiodic density pattern. In Sec. IV we show that wave-packet revivals, essentially a quasiperiodic Talbot effect, are possible, where the initial atomic wave function can be (nearly) recovered. In Sec. V we conclude by discussing the experimental possibilities of observing these quasiperiodic effects in existing cold atom beams and traps.

II. QUASIPERIODIC PATTERNS IN THE RAMAN-NATH APPROXIMATION

An experimental arrangement for producing a quasiperiodic atom density is shown in Fig. 1. Two pairs of off-resonant laser beams of width w intersect at a point along a transversely cooled atomic beam with velocity U_z propagating in the z direction [29]. Alternatively, in a cold atom trap with the trap lasers off, two pairs of laser pulses impinge on the atoms. Assuming the laser beam pairs are detuned from one another, we can ignore the cross terms in the intensity. The atoms are modeled as having two internal states with

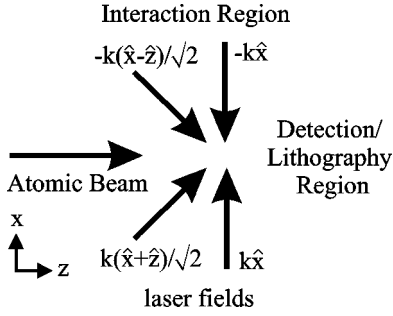


FIG. 1. The atomic beam traverses the quasiperiodic potential formed by the laser beams and is detected by light scattering or lithography after free propagation.

upper-state lifetime Γ^{-1} . The center-of-mass motion is described by plane-wave states. A light-shift potential for the atomic ground state is formed,

$$V(x, z) = V_1(z) \cos 2kx + V_2(z) \cos \sqrt{2}kx, \quad (1)$$

where $V_l(z) \approx \hbar |\Omega_l(z)|^2 / 8\Delta_l$ for Rabi frequencies $\Omega_l(z)$ and atom-field detunings Δ_l of the laser beam pairs $l=1,2$. Spontaneous emission during the atom-field interaction is ignored under the assumption that $|\Omega_l(z)|^2 \Gamma w / 4U_z \Delta_l^2 \ll 1$. This condition assures that the excited state remains essentially unpopulated and has been shown to be important in atomic focusing experiments [6]. The quasiperiodicity arises from the incommensurate wave vectors of the optical potential. Phase stability between the laser fields is essential for the potential's integrity.

While this choice of configuration creates a specific light-shift potential, the arguments that follow can be applied to any potential which contains incommensurate wave vectors. For example, a 2D potential, like the pentagonal Penrose lattice formed by five laser beams intersecting in a plane, could be positioned in front of an atomic beam, or under atoms dropped from a cold trap, to tailor the wave packet. In this sense the optical fields coherently control the quasiperiodic wave packet which forms.

The atomic motion is described by a Schrödinger equation for the transverse wave function $\phi(x, t)$, either in the trap or in the atomic beam's rest frame, $z = U_z t$. Assuming $MU_z^2 \gg \langle MU_x^2 + MU_y^2 + 2V(x, z) \rangle$, one finds [30]

$$i\hbar \frac{\partial \phi}{\partial t} = \left[\frac{p_x^2}{2M} + V(x, t) \right] \phi, \quad (2)$$

where the full, Born-Oppenheimer wave function of the beam is given by

$$\Psi(x, z, t) = \exp\left(i \frac{MU_z}{\hbar} z - i \frac{MU_z^2}{2\hbar} t\right) \phi(x, z = U_z t). \quad (3)$$

The potential in the interaction region appears as a pulse of duration $\tau = w/U_z$ in the atomic rest frame. The pulse shape is determined by the transverse laser profiles.

Three interaction time scales exist: the Raman-Nath [$\tau \ll (\omega_k V_{RN}/\hbar)^{-1/2}$], thick lens [$(\omega_k V_{RN}/\hbar)^{-1/2} \lesssim \tau \lesssim \omega_k^{-1}$], and Bragg-like ($\omega_k \tau \gg 1$) regimes, where $\omega_k = 2\hbar k^2/M$ is a two-photon recoil frequency. Information about the pulse

shape is required to calculate the Raman-Nath parameter, V_{RN} . To present the essential physics of interest here, the quantitative discussion is restricted to the Raman-Nath (thin lens) regime for square pulses,

$$V(x, t) = V(x) = V_1 \cos 2kx + V_2 \cos \sqrt{2}kx \quad \text{for } -\tau < t < 0 \quad (4a)$$

$$= 0 \quad \text{for all other times,} \quad (4b)$$

although computer simulations can be used to solve Eq. (2) for arbitrary interaction times and pulse shapes [31]. For the square pulses $V_{RN} = V_1 + V_2/2$ [32]. In the Raman-Nath approximation the kinetic energy is ignored during the interaction, allowing an immediate integration of Eq. (2) using $\phi(x, -\tau) = 1$. We can write $\phi(x, 0) = \exp[-iV(x)\tau/\hbar]$ or [33]

$$\phi(x, 0) = \exp[i(A_1 \cos 2kx + A_2 \cos \sqrt{2}kx)], \quad (5)$$

where the pulse area is defined by $A_l = -V_l \tau / \hbar$. The standing-wave light fields act as a quasiperiodic atomic phase grating. Equation (5) is valid also for smooth pulse shapes in the Raman-Nath approximation.

After the interaction, the evolution of the wave function into the Fresnel region follows from the free time-dependent Schrödinger equation or its propagator. We can expand Eq. (5) into a plane-wave representation. The resulting, initial wave function for the Schrödinger equation is a superposition of free-particle eigenstates $\exp[ip_{m,n}x/\hbar]$ with energies $E_{m,n} = p_{m,n}^2/2M$, giving the result

$$\begin{aligned} \phi(x, t > 0) = & \sum_{m,n=-\infty}^{\infty} i^{m+n} J_m(A_1) J_n(A_2) \\ & \times \exp\left[i2kx \left(m + \frac{n}{\sqrt{2}}\right) - i\varphi_{m,n}(\omega_k t)\right], \quad (6) \end{aligned}$$

where

$$\varphi_{m,n}(\omega_k t) = E_{m,n} t / \hbar = \left(m + \frac{n}{\sqrt{2}}\right)^2 \omega_k t \quad (7)$$

is the phase associated with the momentum component

$$p_{m,n} = 2\hbar k(m + n/\sqrt{2}), \quad (8)$$

and J_m is a Bessel function. The momentum space wave function superposes a set of regularly spaced, but not periodic, components which are integer combinations of momentum exchanges between the atom and fields. Notice that the wave function has time-independent momentum amplitudes $i^{m+n} J_m(A_1) J_n(A_2)$.

Using a sum rule for Bessel function products, the transverse density, $\rho(x, t) = \phi^*(x, t) \phi(x, t)$, can be written as

$$\rho(x, t) = \sum_{m,n} \rho_{m,n}(\omega_k t) \exp\left[i2kx \left(m + \frac{n}{\sqrt{2}}\right)\right]. \quad (9)$$

The density has time-dependent Fourier amplitudes,

$$\rho_{m,n}(\omega_k t) = J_m \left\{ 2A_1 \sin \left[\left(m + \frac{n}{\sqrt{2}} \right) \omega_k t \right] \right\} \\ \times J_n \left\{ 2A_2 \sin \left[\left(\frac{m}{\sqrt{2}} + \frac{n}{2} \right) \omega_k t \right] \right\}, \quad (10)$$

creating a spatial pattern which evolves in time. Thus, the atomic density is not only a quasiperiodic function of the coordinate x at fixed t but also of the coordinate $z = U_z t$ at fixed x . This exact expression for the density components of a quasiperiodic wave packet, written explicitly for the first time to our knowledge, can be used for direct experimental comparison by properly averaging over the longitudinal and transverse velocity distributions, just as similar results were used for periodic gratings in Ref. [3].

The density Fourier transform (DFT),

$$\rho(q, t) = (2\pi)^{-1} \int \rho(x, t) e^{-iqx} dx \\ = \sum_{m,n} \rho_{m,n}(\omega_k t) \delta(q - p_{m,n}/\hbar), \quad (11)$$

has peaks at $q = p_{m,n}/\hbar = 2k(m + n/\sqrt{2})$ [see Eq. (8)]. When squared, $\rho(q, t)$ gives the time-dependent structure factor of the atomic distribution. The atomic momentum space wave function and the DFT have a dense spacing between components for all times $t \geq 0$ [20,21]. The density is reminiscent of the eigenfunctions of the absolutely continuous spectrum of eigenvalues in the (discrete) Harper model, which are known to exhibit self-similar features up to a correlation length which depends critically on the potential strengths [22,23]. While not part of this work, one could explore the multifractal (scaling) characteristics for such wave functions and density patterns, reflecting the structure of the spectrum and eigenfunctions of the potential (4a) as well as a devil's staircase density of states [27].

In realistic experiments, the δ -function line shape of each spectral component would be broadened by a finite beam width or trap size D . In the Fresnel region for atomic beams wider than the largest important spatial scale [$D \approx 1 - 10 \text{ mm} \gg (A_1 + A_2/\sqrt{2})/2k$], this effect is negligible compared to modifications of the density produced by an initial transverse velocity distribution. For a thermal transverse distribution, $(\pi u_x)^{-1} \exp[-(U_x/u_x)^2]$, with most probable speed u_x , the replacement

$$\rho_{m,n}(\omega_k t) \rightarrow \rho_{m,n}(\omega_k t) \exp[-(p_{m,n} u_x t / 2\hbar)^2] \quad (12)$$

in Eq. (10) rigorously accounts for Doppler dephasing. This expression pertains to atoms in a beam that is laser-cooled in the transverse direction or atoms in a trap or Bose-Einstein condensate after the trapping beams are removed.

In addition, a (single-particle) longitudinal flux distribution, $W(U_z)$, in the atom beam can be incorporated into the calculation. The quantity, $W(U_z) dU_z$, is the probability to find an atom with velocity between U_z and $U_z + dU_z$ passing through a plane perpendicular to the z axis. For the beam atoms detected at a fixed distance $z = U_z t$ from the interaction, the time and pulse areas become velocity-dependent, t

$\rightarrow \bar{t} \bar{U}_z / U_z$ and $A_n \rightarrow \bar{A}_n \bar{U}_z / U_z$, where \bar{t} and \bar{A}_n are referenced to the average velocity, $\bar{U}_z = \langle U_z \rangle$, and longitudinal flux averages are denoted by $\langle \rangle \equiv \int dU_z W(U_z)$. As a result, the velocity-averaged density, $\rho(x, \bar{t}) \equiv \langle \rho(x, t) \rangle$, for a thermal transverse distribution takes the general form

$$\rho(x, \bar{t}) = \sum_{m,n} \exp \left[i2kx \left(m + \frac{n}{\sqrt{2}} \right) \right] \langle \rho_{m,n}(\omega_k \bar{t}) \rangle, \quad (13a)$$

$$\langle \rho_{m,n}(\omega_k \bar{t}) \rangle = \int dU_z W(U_z) \rho_{m,n}(\omega_k \bar{t} \bar{U}_z / U_z) \\ \times \exp\{-[p_{m,n} u_x \bar{t} \bar{U}_z / (2U_z \hbar)]^2\}. \quad (13b)$$

This is an exact quantum expression for the density and its Fourier components, accounting for spherical, chromatic, and transverse aberrations. The expression for $\langle \rho_{m,n}(\omega_k \bar{t}) \rangle$ replaces $\rho_{m,n}(\omega_k t)$ in Eq. (11) for the DFT. To obtain quantitative results, we model the beam's single-particle flux distribution as $W(U_z) = (U_z / \sqrt{\pi} U_0 u_z) \exp[-(U_z - U_0)^2 / u_z^2]$ with $u_z \ll U_0$ and $U_z > 0$. For this narrow flux distribution the average speed is $\bar{U}_z \approx U_0$, and the small relative width is $v \equiv \sqrt{2} \langle U_z^2 - \bar{U}_z^2 \rangle^{1/2} / \bar{U}_z \approx u_z / U_0$ with accuracy $u_z^2 / 2U_0^2$. This distribution is used to find quantitative results below. Note that a longitudinal average is unnecessary in the trap since the pulse duration and evolution time are nearly identical for all of the atoms, $\bar{U}_z \rightarrow U_z \rightarrow 0$.

To detect the density as a function of z , or equivalently $\bar{t} = z / \bar{U}_z$, one can scatter a transient probe off of the atoms to record the time evolution of certain DFT components. For example, a probe pulse with duration $< (ku)^{-1}$ and wave vector $\mathbf{k}_p = -k\hat{x}$ backscatters a field E_{bs} proportional to $\langle \rho_{1,0}(\omega_k \bar{t}) \rangle$ in the $+\hat{x}$ direction:

$$E_{\text{bs}} \sim \int dU_z W(U_z) J_1(2\bar{A}_1 \sin[\omega_k \bar{t} \bar{U}_z / U_z]) \\ \times J_0(2\bar{A}_2 \sin[\omega_k \bar{t} \bar{U}_z / U_z / \sqrt{2}]) \\ \times \exp[-(ku_x \bar{t} \bar{U}_z / U_z)^2].$$

This is a type of free induction decay experiment to detect ground-state population gratings [3,34].

Alternatively, either direct deposition or lithography with the atomic beam could be used to reconstruct the density pattern on a substrate. Atomic lithography has advanced to the point where atoms can be used to carve nanostructures in materials such as silicon, silicon dioxide, and gold [35]. Deposition or the use of lithographic techniques would constitute the creation of a quasiperiodic surface from a coherent atomic density pattern, as opposed to quasiperiodic stacked layers in MBE-type systems [20]. Such quasiperiodic surfaces could be used for solid-state surface and transport studies in metallic and semiconductor samples. The implications for quantum and optical properties may be profound owing to the quasiperiodic boundary conditions for the elec-

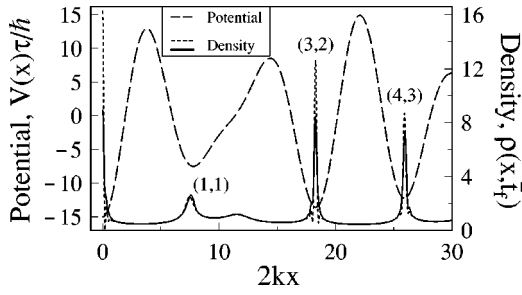


FIG. 2. The optical potential, $V(x)\tau/\hbar = A_1 \cos 2kx + A_2 \cos \sqrt{2}kx$ (— —), is plotted for $A_1 = 5$ and $A_2 = 10$. The corresponding atomic density at the quasifocus, $\rho(x, \bar{t}_f)$, is overlaid for two atomic beam cases. Monovelocity case (- - -): $v = u_x = 0$. Velocity-broadened case (solid line): $v = 0.15$, $\sqrt{2}ku_x/\omega_k = 1$. Quasiperiods are pronounced near $2kx \approx 2\pi ja \approx 2\pi jb\sqrt{2}$, where peaks are labeled by (ja, jb) . The peaks show the sharp features that appear in the density as a result of lensing. (The initial density, equal to one uniformly, defines the relative unit of density. One would multiply the curve by the number of atoms per unit length to find the true density.)

tron or electromagnetic waves, including photon localization and fractal surface states [20,24].

III. QUASIPERIODIC FOCUSING

We now examine two different phenomena in the Fresnel pattern (9) formed by the atoms. Semiclassical dynamics can explain a focusing effect [5]. In Fig. 2 the optical potential (long dashed line) is shown for $\bar{A}_1 = 5$ and $\bar{A}_2 = 10$. With cylindrically focused, Gaussian laser intensities, $\sim \exp[-2(z^2/\sigma_z^2 + y^2/\sigma_y^2)]$, with widths $\sigma_z \approx 30 \mu\text{m}$ and $\sigma_y \approx 5 \text{ mm}$, for example, these pulse areas are achieved for traveling wave powers less than 2 milliwatts in sodium at $\lambda = 589 \text{ nm}$ for $|\Delta| \approx 2 \text{ GHz}$ and $\bar{U}_z \approx 9 \times 10^4 \text{ cm/s}$. Using a circular focus, $\sigma_z \approx \sigma_y \approx 30 \mu\text{m}$, powers of less than 20 microwatts are required in sodium. Each potential well acts as a lens which can focus atoms using the impulsive (dipole) force, $F(x) = M\Delta v_x/\tau = -\partial V(x)/\partial x$, where Δv_x is an impulsive velocity kick. To illustrate this effect, $V(x)$ is Taylor expanded around $x=0$ to give the harmonic focusing force near this point, $F(x) = M\Delta v_x/\tau \approx (4V_1 + 2V_2)kx$. Solving for Δv_x and setting $\bar{t}_{f,\text{cl}} = x/\Delta v_x$, this geometric (classical) argument yields a focus at the time $\omega_k \bar{t}_{f,\text{cl}} = (2\bar{A}_1 + \bar{A}_2)^{-1} = 0.05$ that translates into a spatial distance $z_{f,\text{cl}} = \bar{U}_z \bar{t}_{f,\text{cl}}$. The ratio of pulse areas in Fig. 2, $\bar{A}_2/\bar{A}_1 = 2$, was chosen so that each standing wave contributes an equal semiclassical force. It is possible to show by asymptotic techniques [36] that the true focus can be approximated by $\omega_k \bar{t}_f \approx \omega_k \bar{t}_{f,\text{cl}} [1 + 2.20\omega_k \bar{t}_{f,\text{cl}}(2A_1/3 + A_2/6)^{1/2}]$. For the pulse areas presented here, $\bar{A}_1 = 5$ and $\bar{A}_2 = 10$, this gives a true focus at $\omega_k \bar{t}_f \approx 0.0623$.

We actually evaluate Eq. (13a) at the numerically determined *quasifocus*, where the density peak along $x=0$ is maximized. This gives $\omega_k \bar{t}_f \approx 0.062$ in this case, showing the accuracy of the asymptotic result. The densities plotted in Fig. 2, $\rho(x, \bar{t}_f)$, are symmetric with respect to $x=0$. Results are shown for both a monovelocity beam (small dashed line)

TABLE I. Sequence of approximations for $\sqrt{2}$, $G_s = a_s/b_s$, defines the dominant quasiperiods, $2kx \approx 2\pi ja_s$, and the quasi-Talbot times t_s of Eq. (14).

s	1	2	3	4	5	6
a_s	1	3	7	17	41	99
b_s	1	2	5	12	29	70
$G_s = a_s/b_s$	1	1.5	1.4	1.4167	1.4138	1.4143
$ \sqrt{2} - G_s $	0.41	8.6e-2	1.4e-2	2.5e-3	4.2e-4	7.2e-5
$\omega_k t_s$	4π	4π	20π	24π	116π	140π

having $v = u_x = 0$ and a beam having a distribution of longitudinal and transverse velocities, $v = 0.15$ and $\sqrt{2}ku_x/\omega_k = 1$ (corresponding to the rms single-photon transverse recoil limit), respectively. The high-contrast pattern persists in the velocity-broadened case although the high-frequency (coherent) oscillations near the base of each peak are damped out. Smaller peaks (for example, the peak at $2kx \approx 3 \times 2\pi \approx 2\sqrt{2} \times 2\pi$ in Fig. 2) result from focusing by the shallower wells which occur at the quasiperiods of the potential, where the incommensurate standing waves are nearly in phase. In general, the irrational wave-vector ratio, $\sqrt{2}$ in this case, can be approximated as the ratio a/b , where a and b are positive integers without common factors. Quasiperiods will then be defined by $2kx \approx 2\pi ja \approx 2\pi jb\sqrt{2}$ for any integer j . One particular converging sequence, $G_s = a_s/b_s$, which approximates $\sqrt{2}$, is given in Table I [37]. For this sequence each successive approximation is about five to six times more accurate than the previous approximation.

Several peaks in Fig. 2 are labeled by their values of (ja, jb) . Note that the pair $(ja, jb) = (4, 3)$ in Fig. 2 does not appear in Table I as it is not part of the G_s sequence. The approximation $a/b = 4/3 = 1.\bar{3}$ is not a significantly better approximation to $\sqrt{2}$ than $a_2/b_2 = 3/2$, so a larger phase mismatch in the incommensurate potentials occurs at $2kx = 8\pi$ when compared to $2kx = 6\pi$. The resulting, shallower potential well leads to a smaller density peak at the quasifocus. Generally, for smaller differences between ja and $jb\sqrt{2}$, the quasiperiodicity is more pronounced (i.e., the peaks near $2kx \approx 2\pi ja$ approach the size of the peak at $x=0$). For example, we can find the density peak near the point $2kx \approx 14\pi \approx 10\pi\sqrt{2}$ (not shown in Fig. 2 but corresponding to $s=3$ in Table I and $j=1$) for the velocity-broadened case. The density has a value of 8.907 at the point $2kx = 44.2217 \approx 14.08\pi$ compared to the peak of 8.920 at $2kx=0$. Thus, the focal density underlines the quasiperiodicity of the system.

The DFT, when properly averaged over the velocity distributions, contains the spectral information important for lithography, scattering, or surface science. If we are not interested in the signs of the DFT components, the DFT can be specified by plotting the magnitude of the Fourier amplitudes from Eq. (13b), $|\langle \rho_{m,n}(\omega_k \bar{t}) \rangle|$, at the wave vectors $q = 2k(m+n/\sqrt{2})$. In Fig. 3(a) we compare the magnitudes of the Fourier amplitudes at the focal plane, $|\langle \rho_{m,n}(\omega_k \bar{t}_f) \rangle|$, for the monovelocity (triangular points) and velocity-broadened (square points) cases of Fig. 2. For the given parameters in the velocity-broadened density, $v = 0.15$ and $\sqrt{2}ku_x/\omega_k = 1$, both the magnitude of the Fourier amplitude at each q value

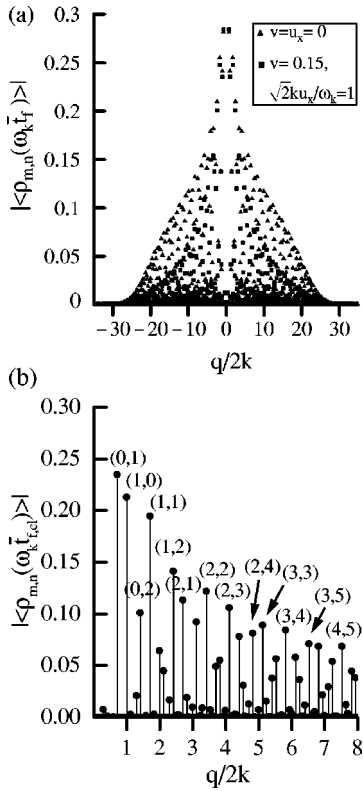


FIG. 3. The magnitude of the density Fourier amplitudes, $|\langle \rho_{m,n}(\omega_k \bar{t}) \rangle|$, plotted at $q=2k(m+n/\sqrt{2})$, as given by Eqs. (10) and (13a). The common amplitude, $\langle \rho_{0,0}(\omega_k \bar{t}) \rangle=1$, is not shown but defines the relative scale for the Fourier components. (a) Comparison between focal amplitudes $|\langle \rho_{m,n}(\omega_k \bar{t}_f) \rangle|$ of the monovelocity case (triangles), $v=u_x=0$, and the velocity-broadened case (squares), $v=0.15$, $\sqrt{2}ku_x/\omega_k=1$. These are the Fourier amplitudes of the focal densities plotted in Fig. 2. The degradation of amplitudes by Doppler decay is evident in the velocity-broadened case. (b) Amplitudes for the monovelocity ($v=u_x=0$) case at the classical focal position, $|\langle \rho_{m,n}(\omega_k \bar{t}_{f,cl}) \rangle|$ (circles). The region of q values shown in (b) contains amplitudes labeled by (m,n) . The horizontal axes for both (a) and (b) are densely packed with small Fourier amplitudes.

and the overall width of the DFT are reduced when compared to the monovelocity case. However, this velocity broadening does not eliminate the strong modulation, as represented by the significant number of Fourier amplitudes (square points) remaining in Fig. 3(a) for $|m|, |n| > 0$. These relatively large Fourier amplitudes at relatively large q are still needed to form the high-resolution focus given by the solid line in Fig. 2.

The Fourier spectra of Fig. 3(a) have qualitative scaling properties: for any Fourier wave vector of the density q_0 , a wave vector $q'=2k(m'+n'/\sqrt{2})$ can be found which is arbitrarily close to q_0 , even if the amplitude of that component is much less than unity. To show these amplitudes in more detail, in Fig. 3(b) we plot the magnitudes of the density Fourier amplitudes in the region $0 < q/2k < 8$ for the monovelocity beam ($v=u_x=0$) evaluated at the classical focal time, $|\langle \rho_{m,n}(\omega_k \bar{t}_{f,cl}) \rangle|$. A few of the larger amplitudes at $q=2k(m+n/\sqrt{2})$ are labeled by their corresponding values of (m,n) . The larger amplitudes are dominated by terms where

both m and n are positive as a result of the properties of the Bessel functions in Eq. (10). Indirect evidence that the true focus of the monovelocity atom beam is not at the classical focal time is given by comparing Figs. 3(a) and 3(b). The magnitude of the amplitude for each q value in Fig. 3(a), the true focus, is generally larger than the amplitude for the same q value at the classical focus in Fig. 3(b).

Using computer simulations, we have also deduced that when the Raman-Nath approximation breaks down, the cusplike shape of the DFT seen in Fig. 3(a) broadens into a plateau at the thick lens focus with a sharp cutoff at some value of q for the given potential strengths. The physics in that thick lens case, relevant for previous atomic focusing and lithography experiments [5], is more complicated as the atoms can come to a focus within the interaction region. However, the density patterns of the thick lens case show features similar to the thin lens case that we are presenting in detail. Therefore, the expectation is that quasiperiodic optical potentials could create high-contrast surfaces in existing atomic focusing geometries if the phase between incommensurate standing wave fields can be maintained.

IV. QUASI-TALBOT EFFECT

Atoms that propagate after interacting with periodic atom optical elements exhibit a self-imaging of their wave function, or Talbot effect, and return to uniform density at times $\omega_k t = 2\pi j$ for integer $j > 0$ [9,10]. While an exact self-imaging which reproduces $\phi(x,0)$ [Eq. (5)] is impossible owing to the dispersion in Eq. (7), the quasiperiodic nature of the wave function can lead to a quasirephasing when $\varphi_{m,n} \approx 2\pi j'$ for some integer $j' > 0$. Initially, we ignore the velocity-averaging process which would destroy this new effect but suggest two ways to overcome this below.

The appropriate observation times for self-imaging will produce phases for each momentum component which are nearly integer multiples of 2π . For even values of b_s , the choice, $\omega_k t_s = 2\pi b_s$, from Eq. (7) gives the phases

$$\varphi_{m,n}(2\pi b_s) = 2\pi(b_s m^2 + b_s n^2/2 + b_s \sqrt{2}mn), \quad (14)$$

where we again refer to Table I, and $b_s \sqrt{2} \approx a_s$ by construction. At these times the first two terms in Eq. (14) are integers for all m,n . Furthermore, the third term is nearly an integer, as required. For odd values of b_s , the rephasing occurs at $\omega_k t_s = 4\pi b_s$.

The wave-function phase $\theta(x,t)$ is defined by $\phi(x,t) = |\phi(x,t)| \exp[i\theta(x,t)]$. For exact self-imaging, this phase returns to $\theta(x,0) = A_1 \cos(2kx) + A_2 \cos(\sqrt{2}kx)$ and the density to unity. In Fig. 4 we plot $\theta(x,t_s)$, as well as the atomic density $\rho(x,t_s)$, for $A_1 = A_2 = 1$ and $s=2, 4$, and 6 . The self-imaging becomes more pronounced at longer times t_s , corresponding to a better approximation of $\sqrt{2}$ by G_s . The average values (denoted by the bar) and standard deviations (denoted by σ) of both the density, $\rho(x,t_s)$, and the phase difference, $\delta_s = \theta(x,t_s) - \theta(x,0)$, are shown in Table II for the cases of Fig. 4. Note that these averages are performed over many periods of both potentials, $|2kx| \leq 16\pi$. The improvements in the self-imaging are evident as $\sigma(\rho(x,t_s))$ and $\sigma(\delta_s)$ converge monotonically to zero as t_s increases.

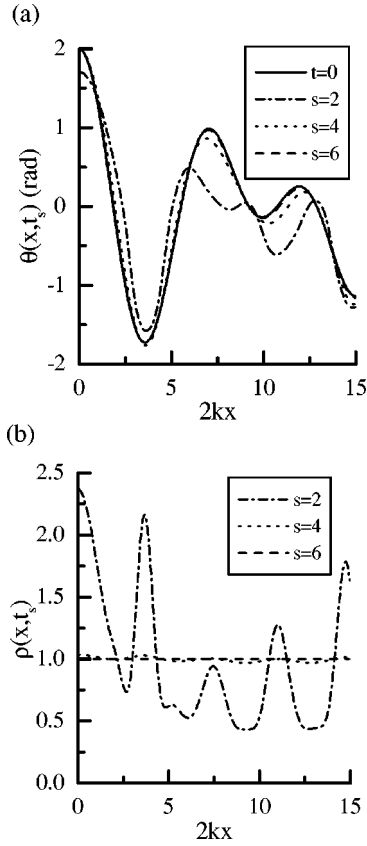


FIG. 4. Quasiperiodic Talbot effect for $A_1=1$ and $A_2=1$. (a) $\theta(x, t_s)$, the phase of the atoms at the quasi-Talbot times t_s for $s=2$ (-.-.-), 4 (....), 6 (- - -), versus $\theta(x, 0)$, the initial phase (—), where $\theta(x, 0) = A_1 \cos(2kx) + A_2 \cos(\sqrt{2}kx)$. The self-image is more precise at longer times. In fact, $\theta(x, t_6)$ is difficult to distinguish from $\theta(x, 0)$. (b) $\rho(x, t_s)$, the density of the atoms at the quasi-Talbot times t_s for $s=2$ (-.-.-), 4 (....), 6 (- - -). Ideally, the atoms achieve a uniform density of 1.

The values and trends in Table II can be understood quantitatively by expanding the wave function's time-dependent phase factor at the quasi-Talbot times,

$$\exp[-i\varphi_{m,n}(2\pi b_s)] \approx 1 + 2\pi imn(a_s - b_s\sqrt{2}) + 2[\pi imn(a_s - b_s\sqrt{2})]^2, \quad (15)$$

where we have added and subtracted the phase, $2\pi imna_s$, from Eq. (14) to extract the small phase mismatch. Inserting this expression into Eq. (6) and using the Bessel function

TABLE II. Averages (denoted by the bar) and standard deviations (denoted by σ) of the quasi-Talbot density, $\rho(x, t_s)$, and phase mismatch, $\delta_s = \theta(x, t_s) - \theta(x, 0)$, for $|2kx| \leq 16\pi$.

s	2	4	6
$\bar{\rho}(x, t_s)$	1.019	1.00085	1.000024
$\sigma(\rho(x, t_s))$	0.505	0.0170	0.000508
$\bar{\delta}_s$ (rads)	0.0324	0.00645	0.00106
$\sigma(\delta_s)$ (rads)	0.417	0.0899	0.0156

property, $2mJ_m(A) = A[J_{m+1}(A) + J_{m-1}(A)]$, one finds that the approximate wave function to lowest order in $(a_s - b_s\sqrt{2})$ is

$$\begin{aligned} \phi(x, 2\pi b_s) &\approx \phi(x, 0) + i\pi A_1 A_2 (a_s - b_s\sqrt{2}) \\ &\times \sum_{m,n=-\infty}^{\infty} i^{m+n} [J_{m+1}(A_1) + J_{m-1}(A_1)] \\ &\times [J_{n+1}(A_2) + J_{n-1}(A_2)] \\ &\times \exp\left[i2kx\left(m + \frac{n}{\sqrt{2}}\right)\right] / 2 \quad (16) \\ &= \phi(x, 0) \{1 + i\pi A_1 A_2 (a_s - b_s\sqrt{2}) \\ &\times [\cos(2 - \sqrt{2})kx - \cos(2 + \sqrt{2})kx]\}. \quad (17) \end{aligned}$$

Thus, the phase difference is found by taking

$$\begin{aligned} \delta_s &\approx \text{Im}[\ln \phi(x, 2\pi b_s) - \ln \phi(x, 0)] \\ &\approx \pi A_1 A_2 (a_s - b_s\sqrt{2}) [\cos(2 - \sqrt{2})kx - \cos(2 + \sqrt{2})kx]. \quad (18) \end{aligned}$$

The average phase difference, $\bar{\delta}_s$, would be zero if we could average over an infinite period, while the standard deviation of the phase difference, $\sigma(\delta_s)$, would be $\pi A_1 A_2 (a_s - b_s\sqrt{2})$. Averaging over the finite window, $|2kx| \leq 16\pi$, gives analytical correction factors and the expressions $\bar{\delta}_s \approx 0.0663\pi A_1 A_2 (a_s - b_s\sqrt{2})$ and $\sigma(\delta_s) \approx 0.978\pi A_1 A_2 (a_s - b_s\sqrt{2})$. These expressions correspond to the values in Table II with errors of 0.76% and 0.5% in $\bar{\delta}_s$ and $\sigma(\delta_s)$, respectively, for $s=6$ and with errors of 4.9% and 0.6%, respectively, for $s=4$. The errors are over 10% for $s=2$. We see that for fixed pulse areas the phase difference to lowest order in $(a_s - b_s\sqrt{2})$ becomes a better approximation at later quasi-Talbot times, corresponding to G_s being a better approximation of $\sqrt{2}$. Equation (18) has also been verified as a function of the pulse areas, A_1 and A_2 , at the fixed quasi-Talbot time $\omega_k t_{s=4} = 24\pi$ and is more accurate for smaller pulse areas, as expected. A similar expression to Eq. (18) can be derived for the density to second order in $(a_s - b_s\sqrt{2})$.

V. CONCLUSION

The ability to perform an experiment on long time scales is limited by transverse cooling considerations and the longitudinal flux width v . The initial transverse velocity width u_x degrades the focusing effect unless a scaled cooling condition, $ku_x/\omega_k \leq (A_1 + A_2/4)^{-3/4}(A_1 + A_2/2)$ [36], is met. This condition prevents transverse effects from broadening the focal spot size. Such broadening has been suppressed by laser cooling for thick lens focusing schemes [5,35]. We have shown in Fig. 2 that, in spite of strong chromatic aberration, effective thin lens focusing can persist for atoms cooled to the recoil limit, where the cooling condition is clearly met. The longitudinal flux width we used, $v=0.15$, is experimentally reasonable while we have also found using thermal longitudinal beams, $v=0.513$, that similar focusing contrasts require approximately twice the laser power. The

relative experimental importance of a narrow transverse velocity distribution over a narrow longitudinal distribution is apparent in the physics of Eq. (13a). The transverse distribution contributes to the average over the sensitive Doppler phases, $p_{m,n}U_x t/\hbar$, leading to a density Fourier component's Gaussian decay, $\exp[-(p_{m,n}u_x t/2\hbar)^2]$, while the longitudinal average over slightly different focal regions for each velocity subclass is a slowly varying integral over the Fourier amplitudes. Atom beams from recent experiments [2,5,38,39], including a beam produced from a Bose-Einstein condensate, could confirm our quasiperiodic focusing results.

For the quasi-Talbot effect to be observable, the beam or trap needs to be cooled below the recoil limit ($ku_x \ll \omega_k$) in the transverse direction. Atomic beams from previous experiments (e.g., Chapman and co-workers in Ref. [10]) with narrow transverse and longitudinal distributions have allowed for an observation of the normal Talbot effect after diffraction of atoms from periodic microfabricated structures. A quasi-Talbot experiment with SW light fields may be possible with the ultracold atom clouds and beams produced from a Bose-Einstein condensate [39,40], where the longitudinal velocity distribution is narrow as well. Evidence for the normal Talbot effect with SW pulses in the Raman-Nath regime has recently been observed in a separated pulse experiment in atoms released from a condensate [41]. To overcome the Doppler dephasing for long times, $\omega_k t \gg 1$, ground-state photon echo configurations employing the methods devised by Cahn and co-workers [3] can be used to examine quasiperiodic effects. We have also developed a

quantum theory of quasiperiodic echoes: the density components vary in time as harmonics of $\omega_k T$ and $\omega_k T/\sqrt{2}$ after the atoms interact with two field zones separated by a time T . This work will be published at a later date.

In summary, this paper has introduced the possibility of quasiperiodic atom optical elements made from laser intensity gratings with incommensurate wave vectors. The quantum, analytical results show that the atomic wave packet becomes a quasiperiodic function, developing momentum components which are similarly incommensurate. The Fresnel density is a function of the time of flight from the diffraction grating. Atoms come to semiclassical quasifoci according to the depth and curvature of the potential wells. The tunable density can survive velocity-averaging and be used for atomic lithography to create quasiperiodic surfaces for condensed-matter studies. Furthermore, ultracold atoms will exhibit a quasi-self-imaging of their wave functions.

ACKNOWLEDGMENTS

The authors would like to thank F. Nori, Q. Niu, G. Georgakis, R. Merlin, and A.G. Rojo for discussions regarding this work. J.L.C. would like to acknowledge the support of Laura Glick and Professor Max Cohen. This work was supported by the National Science Foundation under Grant Nos. PHY-9414020 and PHY-9800981, the U.S. Army Research Office under Grant No. DAAG55-97-0113 and AASERT No. DAAH04-96-0160, and the University of Michigan.

-
- [1] For review articles, see *Atom Interferometry*, edited by P.R. Berman (Academic Press, San Diego, 1997).
- [2] V.P. Chebotayev, B. Dubetsky, A.P. Kazantzev, and V.P. Yakovlev, *J. Opt. Soc. Am. B* **2**, 1791 (1985); O. Carnal and J. Mlynek, *Phys. Rev. Lett.* **66**, 2689 (1991); D. Keith, C.R. Ekstrom, Q.A. Turchette, and D.E. Pritchard, *ibid.* **66**, 2693 (1991); for a review of atomic matter waves diffracted by standing wave light fields, see C.S. Adams, M. Sigel, and J. Mlynek, *Phys. Rep.* **240**, 145 (1994); E.M. Rasel, K. Oberthaler, H. Batelaan, J. Schmiedmayer, and A. Zeilinger, *Phys. Rev. Lett.* **75**, 2633 (1995); Ch. Kurtsiefer, T. Pfau, C.R. Ekstrom, and J. Mlynek, *Appl. Phys. B: Lasers Opt.* **60**, 229 (1995).
- [3] S.B. Cahn, A. Kumarakrishnan, U. Shim, T. Sleator, P.R. Berman, and B. Dubetsky, *Phys. Rev. Lett.* **79**, 784 (1997).
- [4] See B. Young, M. Kasevich, and S. Chu, in Ref. [1].
- [5] G. Timp, R.E. Behringer, D.M. Tennant, and J.E. Cunningham, *Phys. Rev. Lett.* **69**, 1636 (1992); T. Sleator, V. Balykin, and J. Mlynek, *Appl. Phys. B: Photophys. Laser Chem.* **54**, 375 (1992); J.J. McClelland, R.E. Scholten, E.C. Palm, and R.J. Celotta, *Science* **262**, 877 (1993); V. Sandoghdar, U. Drodofsky, Th. Schulze, J. Stuhler, B. Brezger, M. Drewsen, T. Pfau, and J. Mlynek, *J. Mod. Opt.* **44**, 1883 (1997).
- [6] V. Natarajan, R.E. Behringer, and G. Timp, *Phys. Rev. A* **53**, 4381 (1996).
- [7] P.J. Martin, B.G. Oldaker, A.H. Miklich, and D.E. Pritchard, *Phys. Rev. Lett.* **60**, 515 (1988).
- [8] M.K. Oberthaler, R. Abfalterer, S. Bernet, J. Schmiedmayer, and A. Zeilinger, *Phys. Rev. Lett.* **77**, 4980 (1996); S. Bernet, M.K. Oberthaler, R. Abfalterer, J. Schmiedmayer, and A. Zeilinger, *ibid.* **77**, 5160 (1996).
- [9] H.F. Talbot, *Philos. Mag.* **9**, 401 (1836); J.T. Winthrop and C.R. Worthington, *J. Opt. Soc. Am.* **55**, 373 (1965); K. Patorski, *Prog. Opt.* **28**, 1 (1989).
- [10] J.F. Clauser and M.W. Reinsch, *Appl. Phys. B: Photophys. Laser Chem.* **54**, 380 (1992); U. Janicke and M. Wilkens, *J. Phys. II* **4**, 1975 (1994); M.S. Chapman, C.R. Ekstrom, T.D. Hammond, J. Schmiedmayer, B.E. Tannian, S. Wehinger, and D.E. Pritchard, *Phys. Rev. A* **51**, R14 (1995); S. Nowak, Ch. Kurtsiefer, C. David, T. Pfau, and J. Mlynek, *Opt. Lett.* **22**, 1430 (1997).
- [11] N.P. Bigelow and M.G. Prentiss, *Phys. Rev. Lett.* **65**, 29 (1990); C.I. Westbrook, R.N. Watts, C.E. Tanner, S.L. Rolston, and W.D. Phillips, *ibid.* **65**, 33 (1990); for a review of optical lattices, see P.S. Jessen and I.H. Deutsch, *Adv. At., Mol., Opt. Phys.* **37**, 95 (1996).
- [12] P. Verkerk, B. Lounis, C. Salomon, C. Cohen-Tannoudji, J.-Y. Courtois, and G. Grynberg, *Phys. Rev. Lett.* **68**, 3861 (1992); P.S. Jessen, C. Gerz, P.D. Lett, W.D. Phillips, S.L. Rolston, R.J.C. Spreeuw, and C.I. Westbrook, *ibid.* **69**, 49 (1992).
- [13] F.L. Moore, J.C. Robinson, C. Bharucha, P.E. Williams, and M.G. Raizen, *Phys. Rev. Lett.* **73**, 2974 (1994).
- [14] J.C. Robinson, C. Bharucha, F.L. Moore, R. Jahnke, G.A. Georgakis, Q. Niu, M.G. Raizen, and B. Sundaram, *Phys. Rev. Lett.* **74**, 3963 (1995).
- [15] J.-Y. Courtois, S. Guibal, D.R. Meacher, P. Verkerk, and G. Grynberg, *Phys. Rev. Lett.* **77**, 40 (1996).

- [16] C. Jurczak, B. Desruelle, K. Sengstock, J.-Y. Courtois, C. I. Westbrook, and A. Aspect, *Phys. Rev. Lett.* **77**, 1727 (1996).
- [17] R. Dum and M. Olshanii, *Phys. Rev. Lett.* **76**, 1788 (1996); M. Ben Dahan, E. Peik, J. Reichel, Y. Castin, and C. Salomon, *ibid.* **76**, 4508 (1996).
- [18] S.R. Wilkinson, C.F. Bharucha, K.W. Madison, Q. Niu, and M.G. Raizen, *Phys. Rev. Lett.* **76**, 4512 (1996); Q. Niu, X.-G. Zhao, G.A. Georgakis, and M.G. Raizen, *ibid.* **76**, 4504 (1996).
- [19] G. Raithel, G. Birkel, A. Kastberg, W.D. Phillips, and S.L. Rolston, *Phys. Rev. Lett.* **78**, 630 (1997); T. Müller-Seydlitz, M. Hartl, B. Brezger, H. Hänsel, C. Keller, A. Schnez, R.J.C. Spreeuw, T. Pfau, and J. Mlynek, *ibid.* **78**, 1038 (1997); G. Raithel, G. Birkel, W.D. Phillips, and S.L. Rolston, *ibid.* **78**, 2928 (1997).
- [20] P. J. Steinhardt and S. Ostlund, *The Physics of Quasicrystals* (World Scientific, Singapore, 1987); T.J. Fujiwara and T. Ogawa, *Quasicrystals* (Springer-Verlag, Berlin, 1993).
- [21] M. Ya. Azbel, *Phys. Rev. Lett.* **43**, 1954 (1979); B. Simon, *Adv. App. Math.* **3**, 463 (1982); J.B. Sokoloff, *Phys. Rep.* **126**, 1768 (1985); A. Bondeson, E. Ott, and T.M. Antonsen, Jr., *Phys. Rev. Lett.* **55**, 2103 (1985); A.D. Zetisis, C.M. Soukoulis, and E.N. Economou, *Phys. Rev. B* **33**, 4936 (1986).
- [22] A.P. Siebersma and L. Petronero, *Europhys. Lett.* **4**, 597 (1987); H. Hiramoto and M. Kohmoto, *Phys. Rev. B* **40**, 8225 (1989).
- [23] H. Hiramoto and M. Kohmoto, *Phys. Rev. B* **40**, 8225 (1989).
- [24] M. Kohmoto, B. Sutherland, and K. Iguchi, *Phys. Rev. Lett.* **58**, 2436 (1987); M.S. Vasconcelos, E.L. Albuquerque, and A.N. Mariz, *J. Phys.: Condens. Matter* **10**, 5839 (1998).
- [25] M. Tanibayashi, *J. Phys. Soc. Jpn.* **61**, 3139 (1992).
- [26] L. Guidoni, C. Triché, P. Verkerk, and G. Grynberg, *Phys. Rev. Lett.* **79**, 3363 (1997).
- [27] G.A. Georgakis, G. Sundaram, and Q. Niu (unpublished).
- [28] J.L. Cohen and P.R. Berman (unpublished).
- [29] A similar experiment, leading to the same results as derived in this paper, would have the atomic beam traveling perpendicular to the plane of propagation of the four laser beams. The atomic beam would then travel along the y axis of Fig. 1, avoiding possible geometric effects associated with the intersection of the laser and atomic beams in the interaction region.
- [30] Thus, the paraxial wave function ϕ is written in the reference frame of the z -dependent center of mass of the atom beam [see Eq. (3)] and in an interaction representation for the spatially independent internal motions of the ground state of the beam or trapped atoms.
- [31] Our analytical approach to the thin lens approximation avoids the complications of numerical computations in coordinate space, where a lattice would have to be defined underneath a quasiperiodic function and where the width of each Fourier component would be limited by a fast Fourier transform (FFT) spatial sampling window of width L , allowing a resolution of $\Delta k = 2\pi/L$. While propagation of the free wave function from the pulse to later times by a Crank-Nicholson method is inefficient, standard FFT into momentum space after a numerical or analytical coordinate space integration over the pulse creates a mismatch in the quasiperiodic momentum components and leads to disastrous phase errors in calculating the time evolution. Any calculation in the thick lens regime requires a solution of the differential equation, Eq. (2), preferably performed in momentum space from the outset if free-space evolution is to follow the interaction. This avoids the lattice complications. To calculate the wave function and density within the interaction region in the thick lens regime, we have successfully employed the Crank-Nicholson method [see S.E. Koonin, *Computational Physics: FORTRAN Version* (Addison-Wesley, Reading, MA, 1990)].
- [32] C. Henkel, J.-Y. Courtois, and A. Aspect, *J. Phys. II* **4**, 1955 (1994). The Raman-Nath condition restricts the interaction time to $\tau \ll [\omega_k(V_1 + V_2/2)/\hbar]^{-1/2}$. Hence, $V_{RN} = V_1 + V_2/2$. A thin lens condition which should also be maintained here is $\tau \ll [2\omega_k(V_1^2 + V_2^2/2 + \sqrt{2}V_1V_2)/3\hbar^2]^{-1/3}$, assuring that a spatially modulated phase does not develop during the interaction. These conditions were found using a nonperturbative procedure to derive the small-time evolution operator of Eq. (2) and to find the spatially modulated exponential amplitude and phase corrections, respectively, to $\phi(0)$, Eq. (5). While V_{RN} is typically determined by the interaction time τ for which the average kinetic energy of the wave packet in the potential is equal to the minimum interaction strength coupling the momentum components, this definition has less meaning in the quasiperiodic case since it does not correspond to the amplitude modulation of the wave function. We could find this condition as well using Eqs. (3) and (5). The kinetic energy is given by $E_{KE} = -\hbar^2 \langle \phi(0) | \partial^2 / \partial x^2 | \phi(0) \rangle / 2M = \omega_k \tau^2 (V_1^2/2 + V_2^2/4) / \hbar$ while the minimum interaction strength is given by $V_{min} = \min(V_1, V_2)/2$.
- [33] R. Mosseri and F. Bailly, *J. Phys. I* **2**, 1715 (1992).
- [34] B. Dubetsky and P.R. Berman, *Appl. Phys. B: Lasers Opt.* **59**, 147 (1994).
- [35] K.K. Berggren, A. Bard, J.L. Wilbur, J.D. Gillaspay, A.G. Heig, J.J. McClelland, S.L. Rolston, W.D. Phillips, M. Prentiss, and G.M. Whitesides, *Science* **269**, 1255 (1995); S. Nowak, T. Pfau, and J. Mlynek, *Appl. Phys. B: Lasers Opt.* **63**, 203 (1996); K.S. Johnson, K.K. Berggren, A. Black, C. Black, A.P. Chu, N. Dekker, D. Ralph, J.H. Thywissen, R. Younkin, M. Prentiss, M. Tinkham, and G. Whitesides, *Appl. Phys. Lett.* **69**, 2773 (1996).
- [36] J.L. Cohen, B. Dubetsky, and P.R. Berman, *Phys. Rev. A* (to be published).
- [37] The sequence is defined by the recurrence formulas, $a_l = a_{l-1} + 2b_{l-1}$ and $b_l = a_{l-1} + b_{l-1}$ for $a_1 = b_1 = 1$.
- [38] J. Schmiedmayer, M.S. Chapman, C.R. Ekstrom, T.D. Hammond, D.A. Kokorowski, A. Lenef, R.A. Rubenstein, E.T. Smith, and D.E. Pritchard, in Ref. [1], pp. 6 and 7.
- [39] M. Kozuma, L. Deng, E.W. Hagley, J. Wen, K. Helmerson, S.L. Rolston, and W.D. Phillips, *Phys. Rev. Lett.* **82**, 871 (1999).
- [40] M.H. Anderson, J.R. Ensher, M.R. Matthews, C.E. Wieman, and E.A. Cornell, *Science* **269**, 198 (1995); C.C. Bradley, C.A. Sackett, J.J. Tollett, and R.G. Hulet, *Phys. Rev. Lett.* **75**, 1687 (1995); K.B. Davis, M.-O. Mewes, M.R. Andrews, N.J. van Druten, D.S. Durfee, D.M. Kurn, and W. Ketterle, *ibid.* **75**, 3969 (1995); D.G. Fried, T.C. Killian, L. Willmann, D. Landhuis, S.C. Moss, D. Kleppner, and T.J. Greytak, *ibid.* **81**, 3807 (1998).
- [41] S.L. Rolston (private communication).